

Article

Utilizing Sequential Action Control Method in GaN-Based High-Speed Drive for BLDC Motor

Payam Niknejad , Tanushree Agarwal and M. R. Barzegaran * 

Department of Electrical Engineering, Lamar University, Beaumont, TX 77710, USA; pniknejad@lamar.edu (P.N.); tagarwal@lamar.edu (T.A.)

* Correspondence: barzegaran@lamar.edu; Tel.: +1-305-898-9628

Received: 6 October 2017; Accepted: 16 November 2017; Published: 21 November 2017

Abstract: This paper presents a hybrid model-based control algorithm that combines Model Predictive Control (MPC) and Sequential Action Control (SAC) deployed in a high-speed drive for Brushless DC (BLDC) motor by using a DC-DC converter with Gallium Nitride (GaN) switches. GaN FETs are selected because of their higher speed and lower power loss as compared with traditional Si switches. In the proposed framework, SAC processes the initial values of the control variables as well as their time of application and their duration in MPC loop. After receiving the underlying estimation of future contribution from SAC, MPC consolidates it with current input and predicts future control values by using the system state space model. This hybrid control conserves control effort and reduces sensitivity to initial conditions. In this way, converter's output voltage is controlled to produce the reference speed at the motor output. National Instrument PXIe-6356 module is utilized as the interface between software and hardware that is a multi-function, LabVIEW-compatible data acquisition device. The viability of the proposed hybrid optimization for the high-speed drive is confirmed numerically by utilizing MATLAB/Simulink and approved experimentally using a Gallium Nitride (GaN) half-bridge DC-DC converter.

Keywords: BLDC motor; GaN-based converter; high-speed drive; Model Predictive Control (MPC); Sequential Action Control (SAC)

1. Introduction

Advancement in power electronics and control methods have been predominantly guided by engineering applications and powered by the progress attained in technologies like power semiconductors, grid-connected converters, inverters, high-speed drives, and analog and digital electronics. Presently, the control system technology is at an exemplary stage, which requires better control systems that are fast, accommodating, and adaptive to unforeseen conditions, unlike the preceding control systems where the focus was on stabilization and robustness [1–4].

Model Predictive Control (MPC) is a viable option for the control of a power converter since it has a reliable mathematical model that helps in predicting the performance of variables being controlled in electrical and mechanical systems by conferring the future output using present input values and future input values along with the control action. It also permits the inclusion of system constraints and nonlinearities, if any, in the given model [5,6].

Despite the flexibilities MPC offers, the primary value for each loop is a presumption. Initialization for each loop is significant since the nonlinear dynamics indicate that the variable being controlled is non-convex and will yield poor local minima and hence it would not be able to modify itself with the changing conditions [7].

To resolve these challenges, we combine Sequential Action Control (SAC) to existing MPC. SAC finds the single optimal control value for initialization of each loop and decides when to act

and its duration of action. SAC features feedback control and reiteration at each time step until horizon regresses. SAC offers online closed-loop control that is unaffected by the discontinuities in dynamics and makes the system faster. When measured up against its alternatives, it is observed that SAC computes higher bandwidth (1 KHz) closed-loop trajectories at a lower final cost in lesser time (milliseconds/seconds versus hours). Therefore, it can be concluded that SAC provides a model-based response to state capably even for saturated, underactuated, nonlinear, and high dimensional systems [8,9].

In previous works, it has been demonstrated that SAC has proven successful when used in real time closed-loop applications such as robot control for trajectory synthesis [10]. SAC has also been applied in life sciences experiments, where it's crucial to control the unstable equilibria of nonlinear systems, since it conserves control effort, avoids parameter tuning, and reduces sensitivity to initial conditions [11].

The power electronics technology based on silicon and Gallium Nitride (GaN) semiconductors necessitates higher power consumption so that it can dispense higher switching frequency and lower power losses. To accomplish this, we add an LC resonant circuit that provides Zero Voltage Switching (ZVS) and Zero Current Switching (ZCS) as well as filtering the converter's output voltage and output current [2,3]. In addition to this, a system based on Digital Signal Processing (DSP) and Field Programmable Gate Array (FPGA) is required. There are several options available, such as dSPACE, Speedgoat, PXIe-6356, etc. Out of them, National Instrument PXIe-6356 offers a cheaper solution, in which the DSP part is compatible with MATLAB/SIMULINK and the FPGA part is programmed in LABVIEW.

Despite the high efficiency and linear torque-speed characteristics of brushed DC motors, they need regular maintenance like replacing the mechanical commutators. Brushless DC motors (BLDCs) that use a permanent magnet rotor and have other advantages like better dynamic response and higher speed range are good options to solve this problem [12].

In this paper, PXIe-6356 is chosen as the control platform to control the BLDC motor speed. The control system is established on DSP-FPGA because the requirement is high power computation accessible by DSP along with accurate interface provided by the FPGA. A PC interface is used for debugging and commanding.

The rest of the paper is organized as follows. Section 2 proposes the system description and modeling, Section 3 details the control synthesis, Section 4 depicts the algorithms and MATLAB simulation, Section 5 features the experimental test results and finally, Section 6 presents the conclusion.

2. System Description and Modeling

Figure 1 shows the system configuration used in this paper. A Hardware In the Loop (HIL) speed controller scheme by using GaN DC-DC converter and PXIe-6356 data acquisition device as an interface between LabVIEW processing unit and hardware setup is implemented.

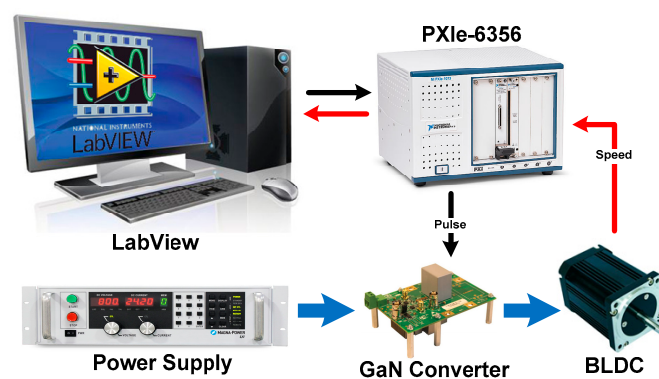


Figure 1. System configuration.

The electrical equivalent circuit of the proposed system is represented in Figure 2. The half-bridge GaN-based DC-DC converter is used as an intermediate level between the power source and BLDC motor to control the armature terminal voltage and consequently the speed of the BLDC motor. Q_1 and Q_2 are GaN switches that are switched complementarily. An LC resonant circuit is used at the converter output to filter the BLDC input current and voltage to assure the zero voltage and zero current switching to decrease the switching power loss [1,4].

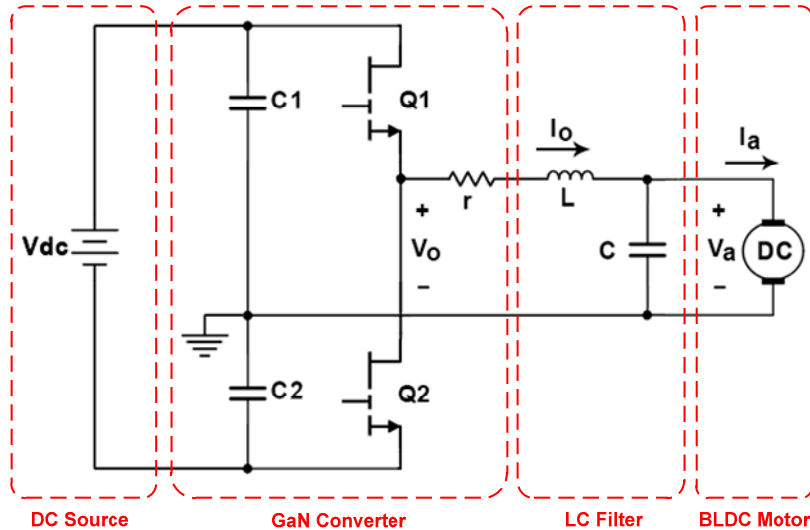


Figure 2. Electrical equivalent circuit.

To model the system, some assumptions are considered. Since the drain-source resistance and internal capacitance of GaN switches are in the order of milliohm and picofarad respectively, they have been neglected and switches are considered as ideal. A small resistant is considered at the converter output which reflects the resistive impedance of the path between the power source and LC filter. If $C_1 = C_2$, the voltage across each of them is $\frac{V_{dc}}{2}$ and (1)–(3) are obtained in which S is the digital switching pulse of the switch Q_1 . When $S = 1$, Q_1 is ON and Q_2 is OFF, and when $S = 0$, Q_1 is OFF and Q_2 is ON.

$$V_o = rI_o + L \frac{dI_o}{dt} + V_a \quad (1)$$

$$V_o = (S - 1) \frac{V_{dc}}{2} \quad (2)$$

$$I_o = C \frac{dV_a}{dt} + I_a \quad (3)$$

To model the BLDC motor, the simple equivalent circuit of Figure 3 is used in which R_a , L_a , and E_a are the armature resistance, armature inductance, and back-emf voltage, respectively. Equations (4)–(7) describe the electromechanical relations in BLDC motor. T_e , T_l , J , and B are electrical torque, load torque, rotor inertia, and friction constant, respectively. ω_m represents the mechanical speed of the motor and K_e and K_t are voltage and torque constants, respectively.

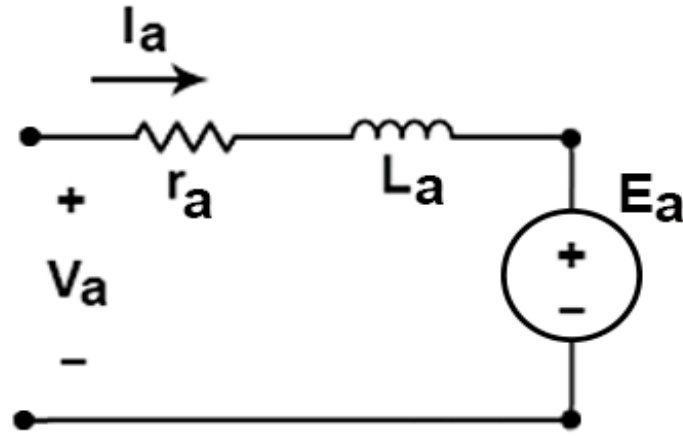


Figure 3. Equivalent circuit of Brushless DC (BLDC) motor.

$$V_a = r_a I_a + L \frac{dI_a}{dt} + E_a \quad (4)$$

$$T_e = J \frac{d\omega_m}{dt} + B\omega_m + T_l \quad (5)$$

$$E_a = K_e \omega_m \quad (6)$$

$$T_e = K_t I_a \quad (7)$$

Hence, the overall state space model of the system can be driven as (8)–(11). By substituting (2), (6), and (7) in these equations, the final model is obtained whose matrix representation is shown by (12).

$$\frac{dI_o}{dt} = \frac{1}{L} V_o - \frac{r_a}{L} I_o - \frac{1}{L} V_a \quad (8)$$

$$\frac{dI_a}{dt} = \frac{1}{L_a} V_a - \frac{r_a}{L_a} I_a - \frac{1}{L_a} E_a \quad (9)$$

$$\frac{dV_a}{dt} = \frac{1}{C} I_o - \frac{1}{C} I_a \quad (10)$$

$$\frac{d\omega_m}{dt} = \frac{1}{J} T_e - \frac{1}{J} T_l - \frac{B}{J} \omega_m \quad (11)$$

$$\frac{d}{dt} \begin{bmatrix} I_o \\ I_a \\ V_a \\ \omega_m \end{bmatrix} = \begin{bmatrix} -\frac{r}{L} & 0 & -\frac{1}{L} & 0 \\ 0 & -\frac{r_a}{L_a} & \frac{1}{L_a} & \frac{K_e}{L_a} \\ \frac{1}{C} & -\frac{1}{C} & 0 & 0 \\ 0 & \frac{K_t}{J} & 0 & -\frac{B}{J} \end{bmatrix} \begin{bmatrix} I_o \\ I_a \\ V_a \\ \omega_m \end{bmatrix} + \begin{bmatrix} S - \frac{1}{2} & 0 \\ 0 & 0 \\ 0 & 0 \\ 0 & -\frac{1}{J} \end{bmatrix} \begin{bmatrix} V_{dc} \\ T_l \end{bmatrix} \quad (12)$$

3. Control Synthesis

MPC has attracted increasing attention in the last decade, especially for power electronic applications because of their discrete nonlinear nature. This method determines the future input of the system by predicting the behavior of the system in a receding horizon based on the system model. State Space (SS) model, Transfer Function (TF) model, Impulse Response (IR) model, and Step Response (SR) model are some types of modeling methods that can be used in MPC [12–15]. The State Space model is used in this paper and is represented by (13) and (14).

$$x_{k+1} = Ax_k + Bu_k \quad (13)$$

$$y_k = Cx_k + Du_k \quad (14)$$

where x , y , and u are controlled variables, output variables, and inputs, respectively and A , B , C , and D are matrices defining the SS model. Subscript k shows a value at k^{th} sampling time [12].

To enhance the performance of the MPC technique, Sequential Action Control (SAC) is added to the existing MPC. The complete control system synthesis of the so-called MPC SAC method, following the cyclic process, is depicted in Figure 4. SAC helps MPC to find the optimal control value by comparing the desired output with the present one using the predefined decision factors as a look-up table (LUT). After the parameter is estimated, the optimal amplitude, time, and duration of the controlled variable are found using a set of algorithms. In this way, SAC calculates the optimal value for MPC implementation.

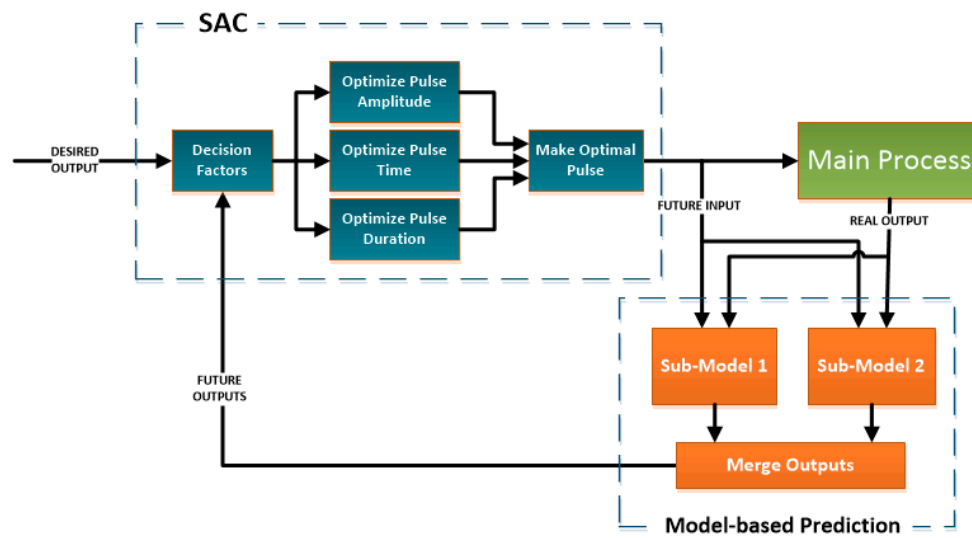


Figure 4. Control system diagram.

At fixed sampling times of every t_s seconds, SAC generates the optimized future input x_{fi} . SAC is a four-step in a loop process that continuously iterates until an optimal minimum is attained that yields x_{fi} . The first step is predicting the initial value x_{init} which begins at t_0 and extends till t_f with a horizon length of $T = t_f - t_s$ when this is performed repeatedly a piecewise continuous response is obtained. The main concept of SAC is shown by (15) where $v(t)$ is the given control variable, $v \in R^m$, a short application duration, $\lambda \in R^+$.

$$x'(t) = f(t, x(t), v(t)) \tag{15}$$

The SS model of the proposed system of this paper is derived from (12)–(16). Since the system is nonlinear, and the model changes when switching status changes, two sub-models are considered. In sub model I, the upper switch (Q_1) is ON, $S = 1$ and the b_{11} parameter of the matrix B is equal to 0.5 and in sub model II, the lower switch (Q_2) is ON, $S = 0$ and the $b_{11} = -0.5$. Sub-models I and II are shown in (16) and (17), respectively. The output variables calculation and prediction are performed by using (16), which is represented by (18) for this system.

Model-based prediction is done with both sub-models, and the absolute value of the error between future predicted outputs and desired output are sent to SAC optimization block to find the value, time to apply, and duration of the controlled variable, which is the S .

$$\frac{d}{dt} \begin{bmatrix} I_L \\ I_a \\ V_a \\ \omega \end{bmatrix} = \begin{bmatrix} -\frac{r}{L} & 0 & -\frac{1}{L} & 0 \\ 0 & -\frac{r_a}{L_a} & \frac{1}{L_a} & \frac{K_e}{L_a} \\ \frac{1}{C} & -\frac{1}{C} & 0 & 0 \\ 0 & \frac{K_t}{J} & 0 & -\frac{B}{J} \end{bmatrix} \begin{bmatrix} I_L \\ I_a \\ V_a \\ \omega \end{bmatrix} + \begin{bmatrix} \frac{1}{2} & 0 \\ 0 & 0 \\ 0 & 0 \\ 0 & -\frac{1}{J} \end{bmatrix} \begin{bmatrix} V_{dc} \\ T_l \end{bmatrix} \tag{16}$$

$$\frac{d}{dt} \begin{bmatrix} I_L \\ I_a \\ V_a \\ \omega \end{bmatrix} = \begin{bmatrix} -\frac{r}{L} & 0 & -\frac{1}{L} & 0 \\ 0 & -\frac{r_a}{L_a} & \frac{1}{L_a} & \frac{K_e}{L_a} \\ \frac{1}{C} & -\frac{1}{C} & 0 & 0 \\ 0 & \frac{K_t}{J} & 0 & -\frac{B}{J} \end{bmatrix} \begin{bmatrix} I_L \\ I_a \\ V_a \\ \omega \end{bmatrix} + \begin{bmatrix} -\frac{1}{2} & 0 \\ 0 & 0 \\ 0 & 0 \\ 0 & -\frac{1}{J} \end{bmatrix} \begin{bmatrix} V_{dc} \\ T_l \end{bmatrix} \quad (17)$$

$$\underbrace{\begin{pmatrix} V_a \\ \omega \\ T_e \end{pmatrix}}_y = \underbrace{\begin{pmatrix} 0 & 0 & 1 & 0 \\ 0 & 0 & 0 & 1 \\ 0 & K_t & 0 & 0 \end{pmatrix}}_C \underbrace{\begin{pmatrix} I_L \\ I_a \\ V_a \\ \omega \end{pmatrix}}_x + \underbrace{\begin{pmatrix} 0 & 0 \\ 0 & 0 \\ 0 & 0 \end{pmatrix}}_{D=0} \underbrace{\begin{pmatrix} V_{dc} \\ T_l \end{pmatrix}}_u \quad (18)$$

4. Simulation

Simulation of the proposed high-speed drive is completed using MATLAB/Simulink along with NI LabVIEW. The model is made in MATLAB/Simulink and then imported in LabVIEW since PXIe-6356 is LabVIEW compatible.

A 60 V DC source paralleled with two series 240 μ F capacitors are used as the DC input to the converter. A half-bridge Converter with GaN switches driven by MPCSAC control unit is built which regulates the DC input voltage into a series of pulses with desired average value. This output is then fed to an LC resonant circuit consisting of a 1 mH pot-core inductor and a 470 μ F bipolar capacitor through a 0.2 Ω resistance to make the current and voltage smoother and help zero voltage and zero current switching in high switching frequencies. To model the GaN FETs, the internal characteristics of existing MOSFETs in the Simulink library such as drain-source ON resistance R_{ON} , internal diode resistance R_D , internal diode forward voltage V_F , and Drain current I_{DS} are modified. The values of these parameters are listed in Table 1.

Table 1. Gallium Nitride (GaN) FET parameters.

Parameter	Value
R_{ON}	50 m Ω
R_D	10 $\mu\Omega$
V_F	6 V
I_{DS}	30 A

The DC Machine block of the MATLAB/Simulink with modified parameters is used to model the desired BLDC motor. Table 2 shows the parameters used for the BLDC modeling.

Table 2. BLDC parameters.

Parameter	Value
Armature Resistance r_a	3.9 Ω
Armature Inductance L_a	0.665 mH
Voltage Constant K_e	0.0087 V \cdot rpm $^{-1}$
Inertia J	0.0007 kg \cdot m 2

The speed waveform of the BLDC Motor along with electrical torque at 100 kHz sampling time for MPCSAC is shown in Figure 5. Initially, the reference speed is 200 rpm for 2 s, then it decreases to -100 rpm (in opposite direction) from $t = 2$ s to $t = 4$ s, and finally goes back to 300 rpm from $t = 4$ s to $t = 6$ s. To evaluate the drive system performance in variable torque condition, a step change of load torque from zero to 2 Nm is applied at $t = 1$ s. It is shown that by using MPCSAC control, the motor real speed follows the reference speed with an acceptable accuracy, and load torque changes do not affect the drive system performance.

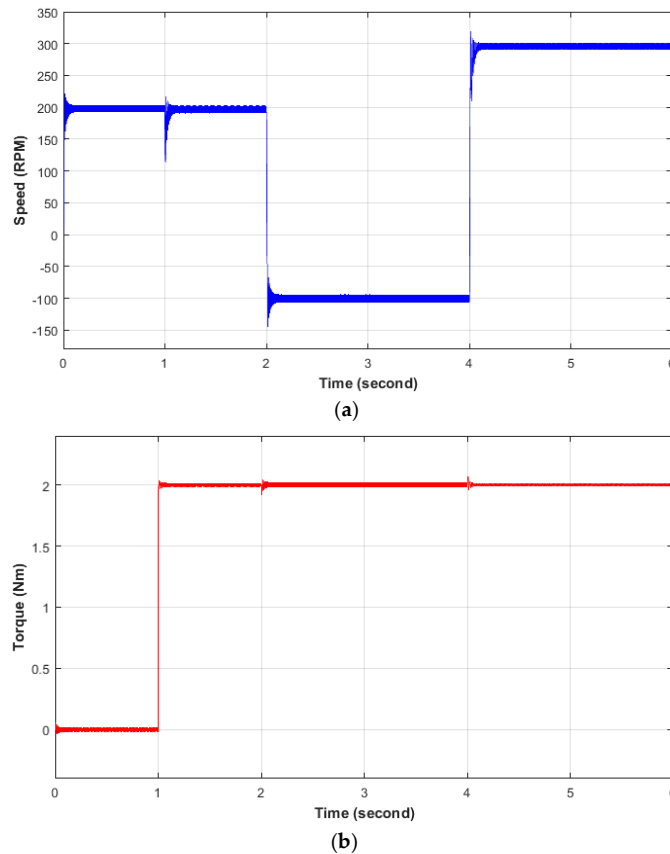


Figure 5. Simulation results: (a) BLDC motor speed (rpm); (b) electrical torque (Nm).

The armature voltage (V_a) and armature current (I_a) of the BLDC are illustrated in Figure 6. Since the basic speed control method is the armature voltage control, variation of the BLDC terminal voltage is very close to the speed variation, while armature current changes are based on load torque, which justifies the torque step change at $t = 1$ s. The average voltage ripple is $\pm 3.46\%$ (compared to the half bridge voltage of 30 V), which is an acceptable value for BLDC motors.

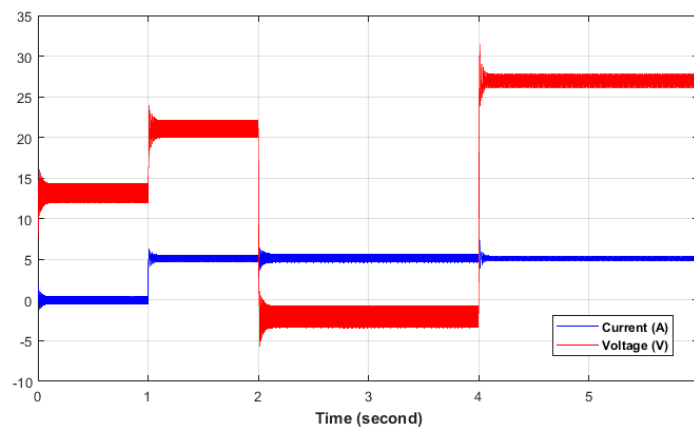


Figure 6. Armature voltage and current of BLDC motor in the simulation.

Figure 7 shows the GaN converter output voltage during simulation time that is including a series of high-speed pulses at 100 kHz switching frequency. A closer look at the pulse width shows that when the desired speed is higher, the pulse width in each switching period is larger, which helps BLDC to increase its speed.

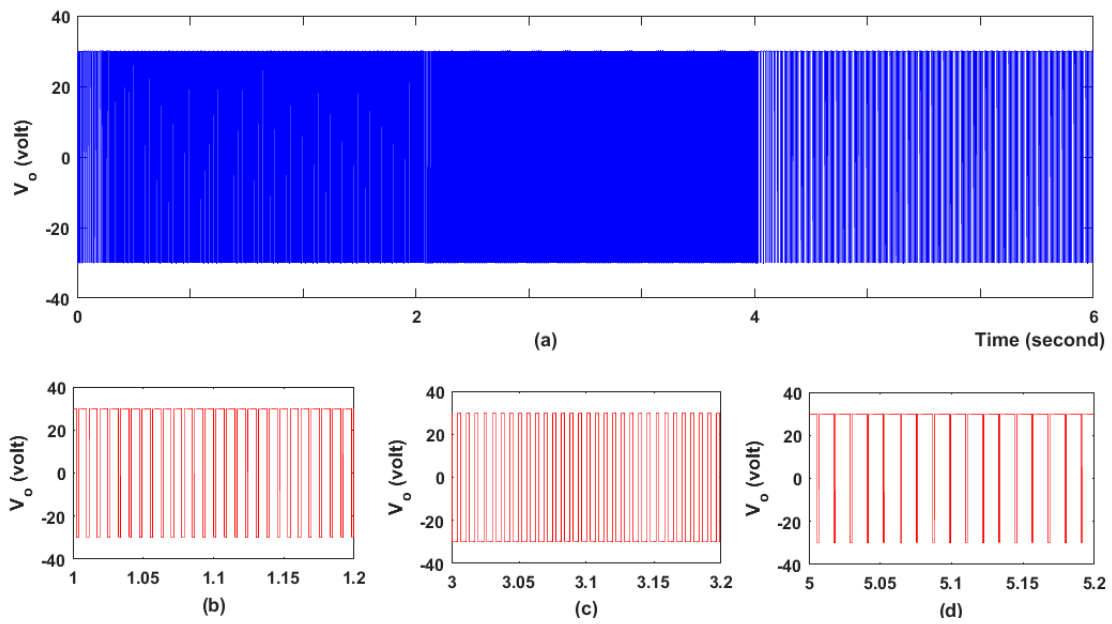


Figure 7. Converter output voltage during: (a) simulation time; (b) 200 rpm reference speed; (c) –100 rpm reference speed; (d) 300 rpm reference speed.

5. Experimental

The experimental setup for the implementation of the proposed drive with MPC-SAC control and the corresponding parameters are shown in Figure 8 and Table 3, respectively. This was an attempt to build a circuit as similar as possible to the simulated system in MATLAB/Simulink. DC input voltage is supplied by Magna-Power XR Series III power supply at 60 V, which supplies the two 240 μF series capacitors as the input source of GaN converter. The GS66508T GaN Module is a 650 V top side cooled board with 30 A, 55 m Ω switches, and a 9–12 V built-in driver circuit is used as the half-bridge DC-DC converter. The output of the GaN converter is connected to an LC filter with $L = 1$ mH and $C = 470$ μF which is further connected to a BLDC motor with parameters listed in Table 2. The speed of the motor is sensed by the sensor and fed to PXIe-6356 simultaneous-sampling, multifunction data acquisition device that offers analog I/O, digital I/O, four 32-bit counters, and analog and digital triggering. LabVIEW software is used as the real-time processor of the system which includes the designed MATLAB/Simulink model and NI-DAQmx software to manage the PXIe-6356. To apply the step change of load torque, a similar BLDC motor is coupled to the motor's shaft and a predetermined reverse voltage is applied to it at $t = 2$ s to resemble the 2 Nm load torque.

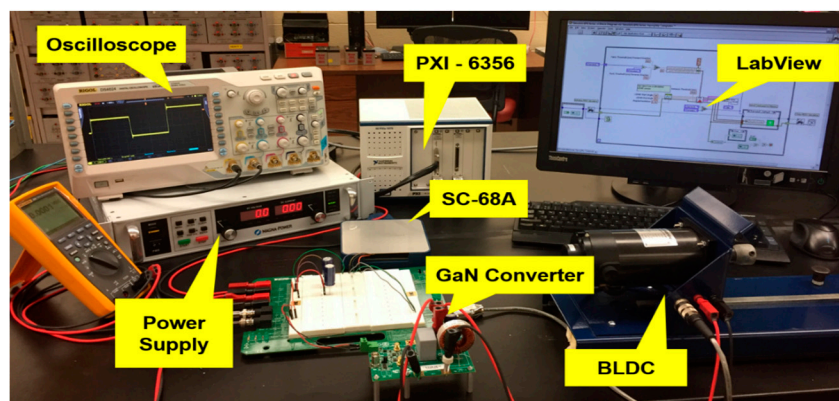


Figure 8. Experimental setup of the proposed system.

Table 3. Experimental parameters.

Parameter	Value
Input Capacitors C_1, C_2	240 μ F
Input DC Voltage V_{dc}	60 V
Filter Inductance L	1 mH
Filter Capacitance C	470 μ F

The model is made in SIMULINK and then imported in LabVIEW using Model Interface Toolkit since PXIe-6356 is LabVIEW compatible. Analog data is collected through PXIe-6356 and SC-68A board that bonds the physical connection between the machine and DAQ. The acquired signals are then analyzed and observed in NI-DAQmx (Measurement and automation system) and go to imported MATLAB/Simulink model in LABVIEW and hence the control is established on the signal. The digital control signal is then sent back to the hardware through NI-DAQmx and PXIe-6356 and SC-68A.

Figure 9 shows the experimental speed control capability of the proposed system along with the electrical torque of the BLDC motor in the lab setup. The reference speed is set to 200 rpm for $t = 0$ s to $t = 2$ s, -100 rpm for $t = 2$ s to $t = 4$ s, and 300 rpm for $t = 4$ s to $t = 6$ s, and the real speed and torque waveforms are monitored and saved by RIGOL DS4024E Digital Oscilloscope. As shown in Figure 9, the speed follows the reference properly and experimental behavior verifies the simulation results.

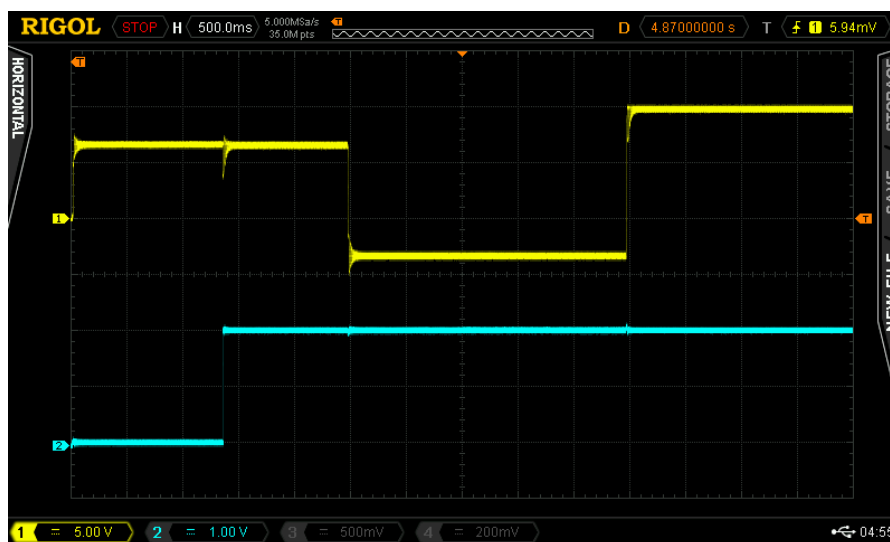


Figure 9. Speed (yellow, x -axis: 400 ms/div, y -axis: 150 rpm/div) and torque (blue, x -axis: 400 ms/div, y -axis: 1 Nm/div) of the BLDC motor in experimental test.

6. Conclusions

A BLDC Motor high-speed drive framework using a GaN-based converter with 100 kHz switching frequency controlled by a hybrid MPC-SAC method is proposed in this paper, and its performance is verified by both simulation and experimental tests. MPC-SAC control technique is an improved Model Predictive Control (MPC) scheme in conjunction with Sequential Action Control (SAC) that predicts and applies the optimal switching pattern to the GaN switches of the DC-DC converter that is capable of high-speed switching and accurate speed control. It also reduces sensitivity to control parameters and initial conditions. Simulation and experimental results have demonstrated that this control strategy progresses the optimal actions together to allow closed-loop, trajectory-constrained control for nonlinear systems. Results show that this HIL approach implements a standard platform for traditional control while enabling measurement incorporation and feedback synthesis at a higher bandwidth than traditional nonlinear moving horizon control schemes. This control scheme is also

compatible with novel technologies with high sampling and switching frequencies. Therefore, it is a viable option for high-speed motor drive application in which real-time and accurate speed control is important.

Acknowledgments: Authors acknowledge the support from center for port management (Texas Legislature).

Author Contributions: M.R. Barzegaran and P. Niknejad conceived and designed the experiments; P. Niknejad and T. Agarwal performed the experiments; P. Niknejad and M.R. Barzegaran analyzed the data; P. Niknejad and T. Agarwal wrote the paper.

Conflicts of Interest: The authors declare no conflict of interest.

References

1. Jones, E.A.; Wang, F.F.; Costinett, D. Review of Commercial GaN Power Devices and GaN-Based Converter Design Challenges. *IEEE J. Emerg. Sel. Top. Power Electron.* **2016**, *4*, 707–719. [[CrossRef](#)]
2. Xue, L.; Boroyevich, D.; Mattavelli, P. Switching condition and loss modeling of GaN-based dual active bridge converter for PHEV charger. In Proceedings of the IEEE Applied Power Electronics Conference and Exposition (APEC), Long Beach, CA, USA, 20–24 March 2016; pp. 1315–1322.
3. Niknejad, P.; Agarwal, T.; Barzegaran, M.R. Using gallium nitride DC-DC converter for speed control of BLDC motor. In Proceedings of the IEEE International Electric Machines and Drives Conference (IEMDC), Miami, FL, USA, 21–24 May 2017; pp. 1–6.
4. Gachovska, T.K.; Gerolami, C. Comparison of Si and GaN-FETs in a VAR compensation application. In Proceedings of the IEEE Electrical Power and Energy Conference (EPEC), Ottawa, ON, Canada, 12–14 October 2016; pp. 1–3.
5. Aleenejad, M.; Mahmoudi, H.; Ahmadi, R. A new modulated model predictive control for permanent magnet synchronous motor. In Proceedings of the IEEE Power and Energy Conference at Illinois (PECI), Champaign, IL, USA, 23–24 February 2017; pp. 1–5.
6. Chen, Z.; Qiu, J.; Jin, M. Adaptive finite-control-set model predictive current control for IPMSM drives with inductance variation. *IET Electr. Power Appl.* **2017**, *11*, 874–884. [[CrossRef](#)]
7. Medjmadj, S.; Diallo, D.; Mostefai, M.; Delpha, C.; Arias, A. PMSM Drive Position Estimation: Contribution to the High-Frequency Injection Voltage Selection Issue. *IEEE Trans. Energy Convers.* **2015**, *30*, 349–358. [[CrossRef](#)]
8. Ansari, A.R.; Murphey, T.D. Sequential Action Control: Closed-Form Optimal Control for Nonlinear and Nonsmooth Systems. *IEEE Trans. Robot.* **2016**, *32*, 1196–1214. [[CrossRef](#)]
9. Nikovski, D.; Esenther, A. Construction of embedded Markov decision processes for optimal control of non-linear systems with continuous state spaces. In Proceedings of the 50th IEEE Conference on Decision and Control and European Control Conference, Orlando, FL, USA, 12–15 December 2011; pp. 7944–7949.
10. Wilson, A.D.; Schultz, J.A.; Ansari, A.R.; Murphey, T.D. Real-time trajectory synthesis for information maximization using Sequential Action Control and least-squares estimation. In Proceedings of the IEEE/RSJ International Conference on Intelligent Robots and Systems (IROS), Hamburg, Germany, 28 September–2 October 2015; pp. 4935–4940.
11. Ansari, A.; Flaßkamp, K.; Murphey, T.D. Sequential action control for tracking of free invariant manifolds. *IFAC-PapersOnLine* **2015**, *48*, 335–342. [[CrossRef](#)]
12. Xia, C.; Li, P.; Li, X.; Shi, T. Series IGBT Chopping Strategy to Reduce DC-Link Capacitance for Brushless DC Motor Drive System. *IEEE J. Emerg. Sel. Top. Power Electron.* **2017**, *5*, 1192–1204. [[CrossRef](#)]
13. Rossiter, J.A. *Model-Based Predictive Control: A Practical Approach*; CRC Press: Boca Raton, FL, USA, 2003.
14. Karamanakos, P.; Geyer, T.; Manias, S. Direct Model Predictive Current Control Strategy of DC–DC Boost Converters. *IEEE J. Emerg. Sel. Top. Power Electron.* **2013**, *1*, 337–346. [[CrossRef](#)]
15. Kouro, S.; Perez, M.A.; Rodriguez, J.; Llor, A.M.; Young, H.A. Model predictive control: Mpc’s role in the evolution of power electronics. *IEEE Ind. Electron. Mag.* **2015**, *9*, 8–21. [[CrossRef](#)]

